APL Materials

Structure-controlled optical thermoresponse in Ruddlesden-Popper layered perovskites

Cite as: APL Mater. 6, 114207 (2018); https://doi.org/10.1063/1.5045782
Submitted: 24 June 2018 . Accepted: 11 October 2018 . Published Online: 26 November 2018

D. Cortecchia, S. Neutzner, J. Yin, T. Salim, A. R. Srimath Kandada, A. Bruno, Y. M. Lam, J. Martí-Rujas, A. Petrozza, and C. Soci

Structure-controlled optical thermoresponse in Ruddlesden-Popper layered perovskites

D. Cortecchia,[1,2,3] S. Neutzner,[3] J. Yin,[4] T. Salim,[5] A. R. Srimath Kandada,[3] A. Bruno,[2] Y. M. Lam,[5] J. Martí-Rujas,[3,6] A. Petrozza,[3,a] and C. Soci[1,7,a]

[1]*Interdisciplinary Graduate School, Nanyang Technological University, Singapore 639798*
[2]*Energy Research Institute @NTU (ERI@N), Nanyang Technological University, 50 Nanyang Drive, Singapore 6375532*
[3]*Istituto Italiano di Tecnologia, Centre for Nano Science and Technology (CNST@PoliMi), Milan 20133, Italy*
[4]*Division of Physical Science and Engineering, King Abdullah University of Science and Technology (KAUST), Thuwal 23955-6900, Kingdom of Saudi Arabia*
[5]*School of Material Science and Engineering, Nanyang Technological University, 50 Nanyang Avenue, Singapore 639798, Singapore*
[6]*Dipartimento di Chimica Materiali e Ingegneria Chimica. "Giulio Natta," Politecnico di Milano, Via Luigi Mancinelli 7, 20131 Milan, Italy*
[7]*Division of Physics and Applied Physics, School of Physical and Mathematical Sciences, Nanyang Technological University, Singapore 637371, Singapore*

(Received 24 June 2018; accepted 11 October 2018; published online 26 November 2018)

Ruddlesden-Popper perovskites are highly attractive for light-emitting and photonic applications. In these exceptionally deformable frameworks, structural properties strongly impact on the energetic landscape of the material; thus, it is crucial to establish a correlation between the structure and optoelectronic characteristics. Here, we study the structural transformations induced by phase transitions in the butylammonium-based series $(BA)_2(MA)_{n-1}[Pb_nI_{3n+1}]$ (n = 1 and n = 2). We show how thermally driven lattice contraction and changes in crystal packing affect their characteristic absorption and photoluminescence. These findings provide new insights for functional perovskites' rational design, highlighting the possibility to tune the structural properties through external stimuli to control their functionalities on-demand.
https://doi.org/10.1063/1.5045782

After revolutionizing the field of solution processed photovoltaics,[1] metal halide perovskites are now flourishing for applications in light emitting and photonic devices such as light emitting diodes (LEDs),[2,3] light emitting field-effect transistors (LE-FETs),[4] and X-ray scintillators and photodetectors.[5–7] Recent advancements in lasing and perovskite nanostructuring are paving the way towards their application as metamaterials and nanophotonic sources.[8–10] The control and understanding of the relationship between the structure and optical properties are required to improve device performance and functionality,[11] and they might lead to the realization of perovskites with dynamically tunable optical response that could be used to achieve new functionalities on-demand.[12–16]

The propensity of the lead halide framework to undergo deformations involving octahedral tilting, distortion, and cation displacement could be exploited to modulate the optoelectronic properties[17–23] upon controlled and reversible structural phase transitions.[24,25] Perovskites of the Ruddlesden-Popper series with formula $(RNH_3)_2(A)_{n-1}[M_nX_{3n+1}]$ ($n \geq 1$) represent an ideal platform since their excitonic and electronic properties, defectivity, bandgap, emission energy, and bandwidth are highly dependent on their crystal structure.[18,20,26–36] These are layered materials which combine a bulky aromatic or aliphatic cation (RNH_3), a small cation A (such as methylammonium or Cs^+), and a metal halide

[a]Authors to whom correspondence should be addressed: csoci@ntu.edu.sg and annamaria.petrozza@iit.it

network of MX_6 octahedra, where M is the divalent metal and X is the halide (F^-, Cl^-, Br^-, I^-). Single layered alkylammonium perovskites $(C_xH_{2x+1}NH_3)_2PbI_4$ (x = 4–18) are known to undergo several first-order phase transitions at low temperature with excellent mechanical resilience.[37–40] However, the impact of multi-layered architecture on the phase transition properties is not well understood, and a thorough correlation between the thermal-induced structural changes and the optical properties is still lacking. In this work, we investigate the BA_2PbI_4 (n = 1) and $BA_2MAPb_2I_7$ (n = 2) perovskites, which are the first two compounds of the series $(BA)_2(MA)_{n-1}[Pb_nI_{3n+1}]$ (where BA = butylammonium and MA = methylammonium), in a wide temperature range, i.e., from 300 K to 77 K, and characterize two new low temperature phases of the n = 2 compound. Using a combination of spectroscopic, structural, and computational analysis, we rationalize the structural changes that impact the optical properties and result in luminescence with a sharp thermal dependence. This shows that thermally activated interconversion of the crystal packing can be effectively exploited to design stimuli responsive luminescent perovskites.

BA_2PbI_4 and $BA_2MAPb_2I_7$ were synthetized by mixing the perovskite precursors (PbI_2, MAI, and butylamine) with the desired stoichiometric ratio in hot hydroiodic(HI) acid aqueous solution. Slow cooling yielded orange and ruby-red plates for BA_2PbI_4 and $BA_2MAPb_2I_7$, respectively, which were used for structural characterization. As previously reported by Billing and Lemmerer,[37] BA_2PbI_4 adopts an orthorhombic structure (*Pbca*) at 293 K [α_{n1}, Fig. 1(a)] while at 223 K, although retaining the same space group, it undergoes a transition involving a significant out-of-plane tilt of the PbI_6 octahedra (D_{out}) from 4.4° to 22.1° with respect to the *ab* plane [β_{n1}, Figs. 1(b) and 2]. Despite the notable change in the Pb-(μ-I)-Pb average angle from 155° to 149°, the PbI_6 units retain a close-to-ideal octahedral geometry in both phases, quantified in terms of octahedral angle variance σ^2_{oct} in Fig. 2. To understand how the change in dimensionality affects the temperature dependence of structural properties, we further studied $BA_2MAPb_2I_7$ by single crystal X-ray diffraction (SC-XRD,

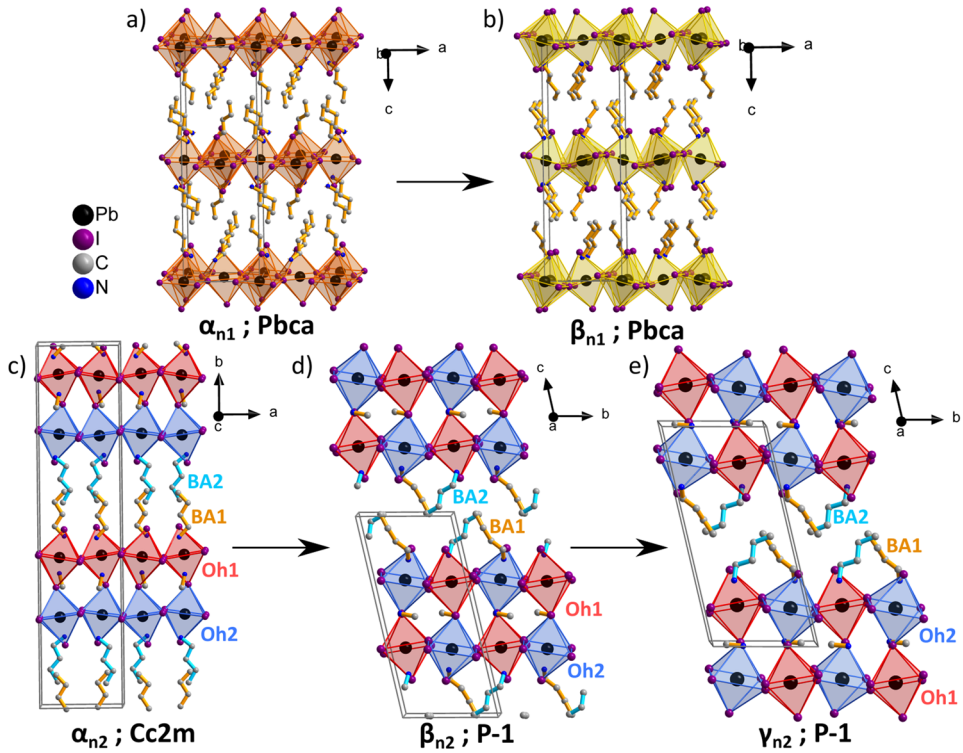

FIG. 1. Phase transitions in the $(BA)_2(MA)_{n-1}[Pb_nI_{3n+1}]$ series. BA_2PbI_4 at (a) 298 K—α_{n1} phase, orthorhombic, Pbca[37] and (b) 223 K—β_{n1} phase, orthorhombic, Pbca.[37] $BA_2MAPb_2I_7$ at (c) 298 K—α_{n2} phase, orthorhombic, Cc2m,[41] (d) 225 K—β_{n2} phase, triclinic, P-1, and (e) 100 K—γ_{n2} phase, triclinic P-1. Oh1 (red) and Oh2 (blue) indicate the octahedra with different tilt and distortion, while BA1 (orange) and BA2 (light blue) indicate the butylammonium cations with different tilt with respect to the inorganic plane.

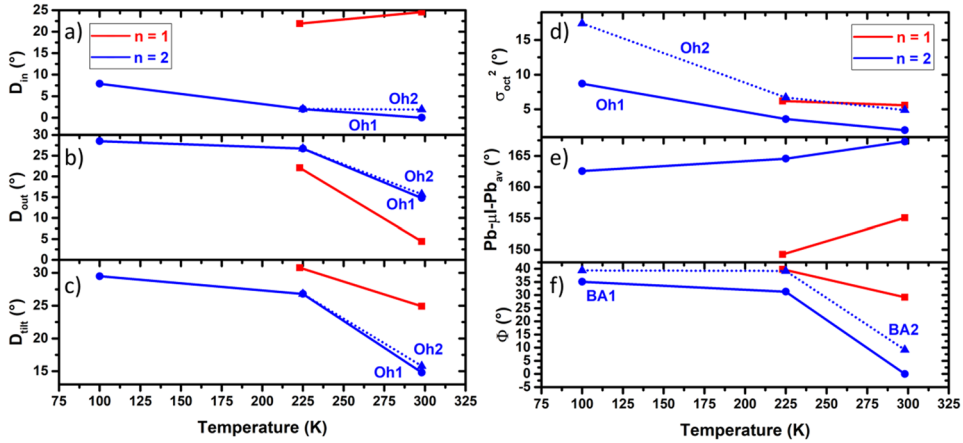

FIG. 2. Thermal evolution of perovskite structural parameters: red = BA_2PbI_4 (n = 1); blue = $BA_2MAPb_2I_7$ (n = 2). Tilt values relative to the smallest Pb-(μ-I)-Pb angle: (a) D_{in} = in-plane tilt; (b) D_{out} = out-of-plane tilt; and (c) $D_{tilt} = 180° - $ (Pb-(μ-I)-Pb).[21] (d) Octahedral angle variance $\sigma^2_{oct} = \frac{1}{11}\sum_{i=1}^{12}((I-Pb-I)_i - 90)^2$.[42] (e) Average bridging angle (Pb-(μ-I)-Pb)$_{av}$. (f) ϕ is the angle between a plane through the lead atoms of the inorganic layer and a vector connecting the first and the last atom of each BA chain.

Table S1 of the supplementary material). At 298 K, the n = 2 compound adopts an orthorhombic structure and space group *Cc2m* (α_{n2}), in good agreement with previous studies.[41] Here, inorganic slabs are formed by two consecutive layers of PbI_6 octahedra sharing the corners in the equatorial position (*ac* plane) and one corner in the apical position (along the *b*-axis); these are alternately stacked with BA^+ bilayers. Different from the n = 1 compound, where all the PbI_6 octahedra are equivalent, the inorganic lattice of $BA_2MAPb_2I_7$ can be divided into two groups of PbI_6 units (Oh1 and Oh2), with Oh1 characterized by smaller octahedral distortion and tilt with respect to Oh2 (see Figs. 1 and 2). In α_{n2}, Oh1 and Oh2 segregate at the opposite sides within an inorganic slab creating a stack of layers with different structural properties along the *b*-axis [Fig. 1(c)]. Lowering the temperature, the crystal point-group symmetry lowers to the triclinic system (space group *P*-1) which characterizes both the β_{n2} and γ_{n2} phases at 225 K and 100 K, respectively [Figs. 1(d) and 1(e)]. In all the three phases, adjacent inorganic layers are staggered relative to each other. However, in the β_{n2} and γ_{n2} phases, the inorganic framework rearranges into a pattern where Oh1 and Oh2 alternate in the *ab* plane as well as along the *c*-axis [Figs. 1(d) and 1(e)]; while keeping different σ^2_{oct} values for Oh1 and Oh2, this configuration levels out their tilt parameters to a unique value (Fig. 2). These structural transformations account for the decrease in the Pb-(μ-I)-Pb average angle from 167.31° to 162.57° and accompany the increase in octahedral tilt (D_{tilt}) at low-temperature, largely driven by the increase in D_{out} compared to the in-plane tilt (D_{in}) (see Fig. 2). We note that, while the $\alpha_{n2} \rightarrow \beta_{n2}$ involves a significant D_{out} increase from 14.8° (15.7°) to 26.7°, $\beta_{n2} \rightarrow \gamma_{n2}$ proceeds with a minimal increment from 26.7° to 28.5°. The changes in the Pb-I framework are templated by *n*-butylammonium, which mirrors the octahedral tilt in the corresponding structures (Fig. 1). In particular, $BA_2MAPb_2I_7$ is characterized by two types of butylammonium cations (BA1 and BA2) having different tilt compared to the inorganic plane. We quantify the geometry of the cation by means of ϕ, defined as the angle between a plane through the lead atoms of the inorganic layer and a vector connecting the first and the last atom of each BA chain (e.g., N1 and C4). In both n = 1 and n = 2 compounds, ϕ increases at low temperature in close correlation with D_{out} (Fig. 2). See also Table S2 of the supplementary material for the summary of the thermal evolution of the structural parameters.

The thermal dependence of the perovskite structure was studied by wide-angle X-ray scattering (WAXS), which is akin to powder X-ray diffraction (PXRD), of the ground crystals. The WAXS of BA_2PbI_4 [Fig. 3(a)] shows a sharp change between 268 and 273 K in the heating cycle (238-243 K in the cooling cycle, Fig. S1 of the supplementary material), consistent with the transition $\beta_{n1} \rightarrow \alpha_{n1}$. Similarly, WAXS of $BA_2MAPb_2I_7$ [Fig. 3(b)] shows two evident changes for $\gamma_{n2} \rightarrow \beta_{n2} \rightarrow \alpha_{n2}$ at 193-198 K and 278-283 K during heating (148-153 K and 283-278 K during cooling, Fig. S1 of the supplementary material), with a more pronounced shift of the diffraction peaks during $\beta_{n2} \leftrightarrow \alpha_{n2}$ due

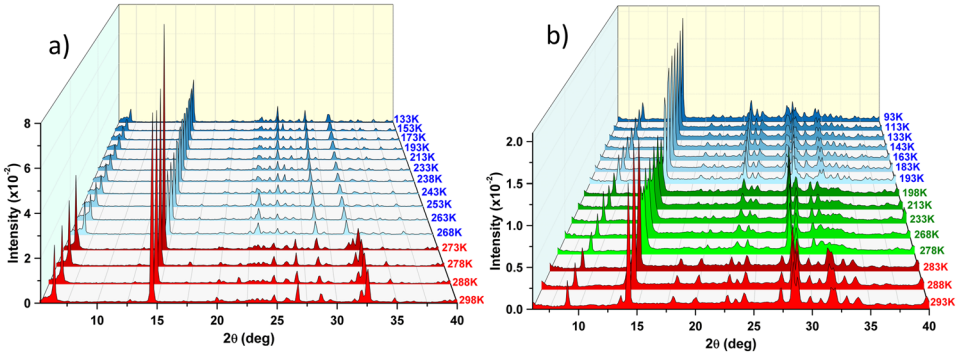

FIG. 3. Temperature dependent P-XRD. (a) BA_2PbI_4: red = α_{n1}, blue = β_{n1}. (b) $BA_2MAPb_2I_7$: red = α_{n2}, green = β_{n2}, blue = γ_{n2}.

to the change in point-group symmetry upon phase transition (Fig. S1 of the supplementary material). The phase transition parameters determined from X-ray characterization are listed in Table I.

The temperature dependence of the lattice parameters was determined by Pawley fit of the powder diffraction patterns (Fig. 4, and Figs. S2–S4 of the supplementary material). BA_2PbI_4 undergoes a marked expansion of the c-axis of 1.3 Å at 270 K, accompanied by a smaller elongation of the a-axis (Δa = 0.4 Å) and shortening of the b-axis (Δb = 0.3 Å). Such widening of the interplanar distance along the c-axis is necessary to accommodate the marked decrease in D_{out} and ϕ. In the case of $BA_2MAPb_2I_7$, the $\gamma_{n2} \rightarrow \beta_{n2}$ at 195 K proceeds with a minimal change in the lattice parameters, confirming the small changes observed from SC-XRD. On the other hand, at 280 K, $\beta_{n2} \rightarrow \alpha_{n2}$ from the triclinic to orthorhombic structure causes a massive elongation of the b-axis (Δb = 30 Å) and shortening of the c-axis (Δc = 11.2 Å). Overall, the phase transitions proceed with expansion of the unit cell at higher temperature, with a marked volume increase in $\beta_{n1} \rightarrow \alpha_{n1}$ (ΔV = 100 Å^3) and $\beta_{n2} \rightarrow \alpha_{n2}$ (ΔV = 1600 Å^3). Consistent with SC-XRD, we observed a minimal volume increase (ΔV = 25 Å^3) for $\gamma_{n2} \rightarrow \beta_{n2}$ of $BA_2MAPb_2I_7$. It is clear from the analysis that the degree of volume contraction dictates the stability and the extent of the perovskite tilt system.

The reversibility of the structural changes is evident from differential scanning calorimetry (DSC) where they appear as typical enantiotropic first-order solid-state phase transitions (Fig. 5). In BA_2PbI_4, a large endothermic peak at 275 K for $\beta_{n1} \rightarrow \alpha_{n1}$ and an exothermic peak at 254 K for $\alpha_{n1} \rightarrow \beta_{n1}$ are observed, with the enthalpy of transition of 10.9 J/g and 8.7 J/g, respectively. The increase in perovskite dimensionality of $BA_2MAPb_2I_7$ lowers the enthalpy of transition to about 5 J/g and shifts the transition to higher temperatures, 284 K for $\beta_{n2} \rightarrow \alpha_{n2}$ and 280 K for $\alpha_{n2} \rightarrow \beta_{n2}$. Due to the limited temperature range, it was not possible to probe the second transition $\gamma_{n2} \leftrightarrow \beta_{n2}$. Although the higher enthalpy shows that the phase transition is more energetically favorable in the n = 1 compound, the much larger thermal hysteresis indicates a higher kinetic energy barrier which slows down the structural rearrangement.[43]

The changes induced by the phase transitions have important consequences on the optical properties of the materials, which were studied on perovskite thin films (Fig. S5 of the supplementary material). At 78 K, BA_2PbI_4 shows an absorption continuum below 450 nm accompanied by a

TABLE I. Phase transition parameters determined from temperature-dependent PXRD (cooling/heating rate 3 K/min).

Formula	Phase	Crystal system	Space group	Transition T ± 2.5 (K) (heating)	Transition T ± 2.5 (K) (cooling)
BA_2PbI_4	α_{n1}	Orthorhombic	*Pbca*	...	240.5 ($\alpha_{n1} \rightarrow \beta_{n1}$)
	β_{n1}	Orthorhombic	*Pbca*	270.5 ($\beta_{n1} \rightarrow \alpha_{n1}$)	...
$BA_2MAPb_2I_7$	α_{n2}	Orthorhombic	*Cc2m*	...	280.5 ($\alpha_{n2} \rightarrow \beta_{n2}$)
	β_{n2}	Triclinic	*P*-1	280.5 ($\beta_{n2} \rightarrow \alpha_{n2}$)	150.5 ($\beta_{n2} \rightarrow \gamma_{n2}$)
	γ_{n2}	Triclinic	*P*-1	195.5 ($\gamma_{n2} \rightarrow \beta_{n2}$)	...

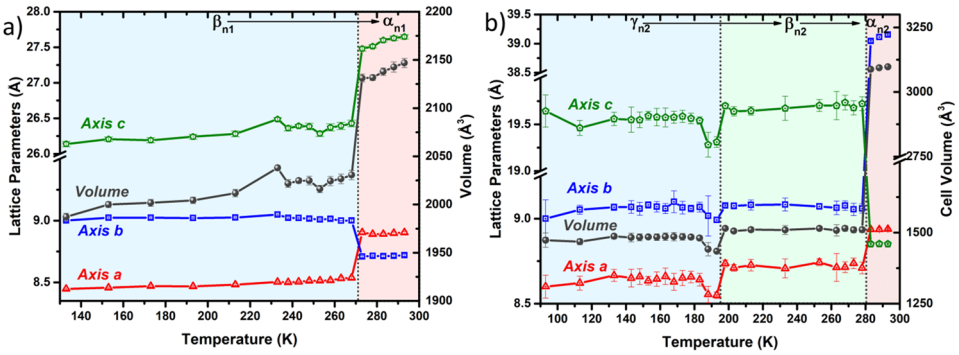

FIG. 4. Perovskite lattice parameters extracted from Pawley fit of the powder WAXS: (a) BA_2PbI_4 and (b) $BA_2MAPb_2I_7$.

strong excitonic absorption feature peaking at 484.1 nm.[26] This band progressively red-shifts and broadens upon increasing temperature, until $\beta_{n1} \rightarrow \alpha_{n1}$ at 275 ± 5 K causes an abrupt red-shift of 24.7 nm as well as a sudden narrowing of ~3 nm [Fig. 6(a), and Figs. S6 and S7 of the supplementary material]. The excitonic absorption is characterized by an evident fine structure in the β_{n1} phase and by an asymmetric line shape in the α_{n1} phase (Fig. S6 of the supplementary material), consistent with the exciton-polaron spectral structures that we have previously discussed in this class of 2D perovskites.[44–46] In $BA_2MAPb_2I_7$ [Fig. 6(c)], only a weak red-shift over a broad temperature range was observed for $\gamma_{n2} \rightarrow \beta_{n2}$, while the transition $\beta_{n2} \rightarrow \alpha_{n2}$ causes a small albeit clear ~3 nm shift [Fig. 6(c), and Figs. S6 and S7 of the supplementary material].

To investigate the structural effects on the optical response, we performed density functional theory (DFT) calculations. Starting from the experimental crystal structures, we optimized the lattices and atomic positions at the GGA/PBE level. The resulting crystal parameters, bandgaps, and band structures are given in Table S3, Table S4, and Fig. S8 of the supplementary material, respectively. Using the many-body perturbation theory at the level of G_0W_0 and Bethe-Salpeter equations (BSEs) to take into account electron-hole interactions, we could reproduce inter-band transitions by involving 32 valence and 32 conduction bands (see Fig. S8 of the supplementary material) as well as the excitonic peak [Figs. 6(b) and 6(d)]. Note that we did not include spin-orbit coupling (SOC) in the G_0W_0 + BSE calculations because of the large computational cost for such large 2D hybrid systems

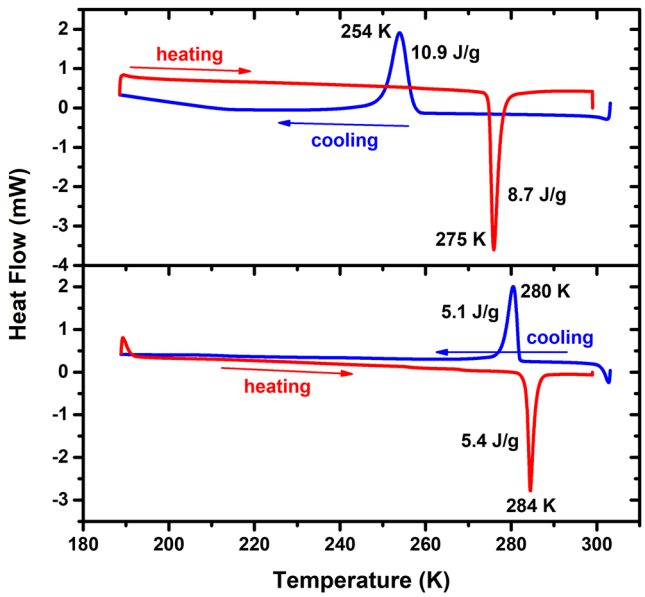

FIG. 5. Differential scanning calorimetry (DSC) of BA_2PbI_4 (upper panel) and $BA_2MAPb_2I_7$ (lower panel).

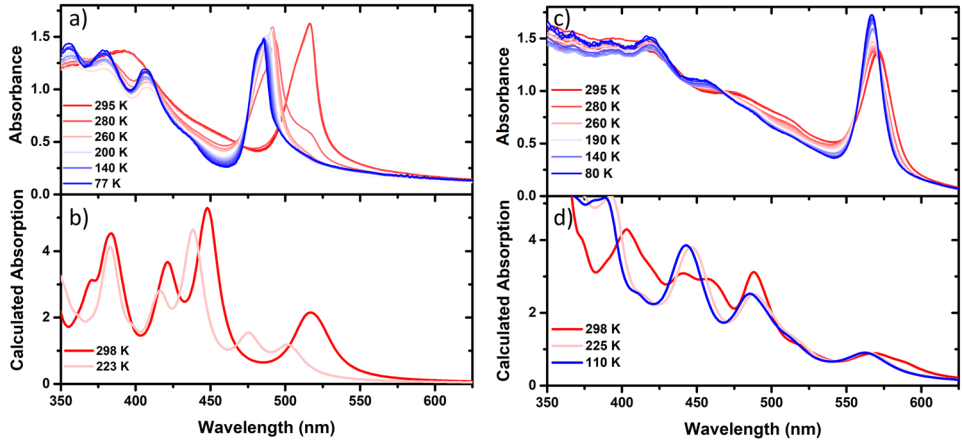

FIG. 6. Temperature dependent experimental absorption of (a) BA_2PbI_4 and (c) $BA_2MAPb_2I_7$. Calculated absorption coefficients of (b) BA_2PbI_4 (α_{n1} and β_{n1}) and (d) $BA_2MAPb_2I_7$ (α_{n2}, β_{n2} and γ_{n2}) at the GGA/PBE level using the G_0W_0 + BSE method.

containing 150-200 atoms. We find that the PBE functional without SOC can reproduce well the bandgaps of BA_2PbI_4 and $BA_2MAPb_2I_7$, while PBE with SOC retains the band curvatures and band degeneracies but only reduces the bandgaps (see Fig. S8 of the supplementary material). The position of the valence band maximum (VBM) is determined by the overlap of Pb-6s and I-5p antibonding atomic orbitals; distortions of the Pb-I-Pb angle from the linear geometry result in poorer orbital overlap, shifting VBM to higher energy and leading to bandgap widening.[47,48] The consequences of this are directly seen from the calculated bandgaps, which decrease from the low to high temperature phases (Fig. S8 of the supplementary material). Similarly, the sudden increase in octahedral tilt (D_{out}) upon phase transition also causes the discontinuous redshift of the excitonic absorption; the calculated absorption spectra well reproduced the trend induced by this structural change, although we note that the calculated spectral shift is less marked than the one observed experimentally (Fig. 6). In addition to this sharp transition, BA_2PbI_4 also undergoes a continuous spectral red-shift with the increase in temperature (Fig. 6, and Figs. S6 and S7 of the supplementary material), which is contrary to the trend observed in $MAPbI_3$, where the bandgap blue-shifts with the increase in temperature (Fig. S9 of the supplementary material).[49] This behaviour of the 3D perovskite was previously attributed to the thermal expansion of the PbI_6 octahedra, which also leads to a reduced Pb-6s/I-5p orbital overlap.[50,51] Although BA_2PbI_4 also evolves towards a slight expansion of the lattice, the absence of the apical coordination of the lead halide octahedra gives them more rotational freedom with respect to the 3D perovskite framework. Therefore, in the 2D perovskite, the volume expansion of the unit cell proceeds with a reorganization of the tilt of the PbI_6 and BA units rather than involving a considerable octahedral expansion, leading to the progressive bandgap narrowing. In comparison with our previous studies on $(PEA)_2PbI_4$ (PEA = phenethylammonium),[46] we note that this is not a general trend of 2D perovskites but is rather related to the characteristic thermal evolution of the crystal structure induced by the specific templating cation. On the other hand, the increase of dimensionality in $BA_2MAPb_2I_7$ leads to an intermediate case where, within the temperature stability range of each phase, the shift of the excitonic peak with temperature is negligible. This correlates well with the structural analysis, showing that the unit cell parameters remain nearly constant within the stability range of each phase, which indicates a more difficult structural reorganization in the multidimensional structure due to increased steric constraints.

Photoluminescence (PL) properties are also very sensitive to structural conformations. Polycrystalline films of BA_2PbI_4 showed phase coexistence up to 293 K, during which the PL band at 493 nm (β_{n1}) gradually converts to the one at 517 nm characteristic of α_{n1} [Fig. 7(a)], indicating that different crystalline domains undergo the phase transition at slightly different rates. The excitonic emission of β_{n1} develops into a highly structured spectral line shape (Fig. S10 of the supplementary material); we have previously suggested that the exciton fine structure may be a consequence of polaronic

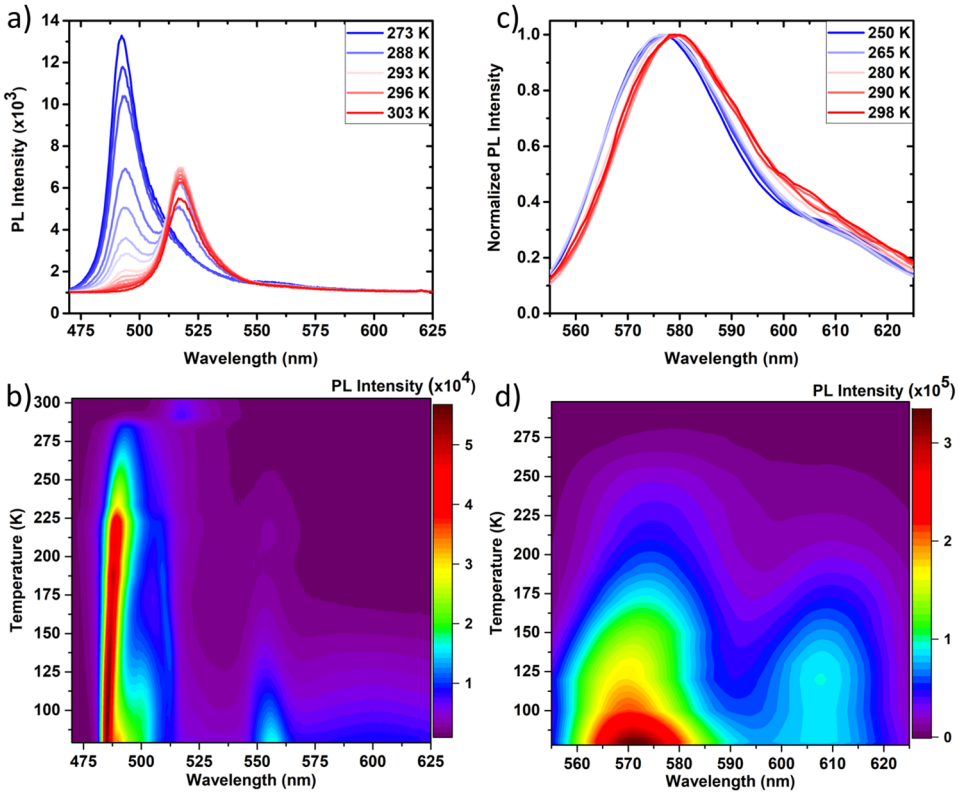

FIG. 7. Temperature dependent photoluminescence (PL) of [(a) and (b)] BA_2PbI_4 and [(c) and (d)] $BA_2MAPb_2I_7$.

effects, arising from the highly polar nature of the lead halide framework, where excitons with distinct lattice-coupling co-exist.[44–46] In addition, a broadband emission peaked at 600 nm becomes relevant below 160 K (Fig. S10 of the supplementary material). We note that even though the change in D_{out} has a dramatic effect on the energy of the excitonic emission, it does not directly affect the onset of such broad luminescence. The activation energy of 35.8 meV (see Fig. S11 of the supplementary material) points towards the formation of sub-bandgap trap states which might relate to exciton self-trapping and the formation of iodide-based defects.[52–54] On the other hand, the luminescence spectrum of the multidimensional film is characterized by two partially overlapping peaks centered at 572 nm and 604 nm, which become evident at low temperature [Figs. 7(c) and 7(d)]. These bands belong to the excitonic emission of $BA_2MAPb_2I_7$ and $BA_2MA_2Pb_3I_{10}$ and indicate the formation of heterogeneous phases with inclusions of the n = 3 compound of the series $(BA)_2(MA)_{n-1}[Pb_nI_{3n+1}]$ (also confirmed from the XRD analysis, Fig. S5 of the supplementary material).[55] Principal component fitting allows us to study the temperature dependence of the n = 2 phase: while $\gamma_{n2} \leftrightarrow \beta_{n2}$ only caused minimal PL changes preventing the clear identification of the transition, $\beta_{n2} \rightarrow \alpha_{n2}$ causes the narrowing of the PL emission (1-2 nm) and its redshift of 2.4 nm (Fig. S7 of the supplementary material). These observations further demonstrate how thermal interconversion of the crystal structure can be exploited to finely shape the energetic landscape of the material.

In conclusion, we thoroughly characterized the thermal dependence of the structural properties of the first two compounds of the Ruddlesden-Popper series $(BA)_2(MA)_{n-1}[Pb_nI_{3n+1}]$ and solved the crystal structure of the β_{n2} and γ_{n2} triclinic phases of $BA_2MAPb_2I_7$. Regardless of the dimensionality, the perovskites showed volume expansion at higher temperature, which drives the decrease in out-of-plane tilt (D_{out}) of the PbI_6 octahedra. We identify D_{out} as the main parameter affecting the excitonic absorption and luminescence energy, and we directly show the importance to achieve control over the octahedral tilt to fine tune the optoelectronic properties. We note that the tendency of the $\beta \rightarrow \alpha$ transition to occur close to room temperature in alkylammonium perovskites enables the control of structural and optical properties by small changes in the temperature. This approach might therefore

be exploited for the realization of all-optical switching photonic devices,[15] or to design more efficient heterogeneous systems for light emitting applications.[9,56,57]

See supplementary material for the description of experimental methods, Figs. S1–S11, and crystallographic information files.

This work was supported by the Ministry of Education (Ref. Nos. MOE2016-T1-1-164 and MOE2011-T3-1-005) and the National Research Foundation (Ref. No. NRF-CRP14-2014-03) of Singapore. We thank the financial support from the EU Horizon 2020 Research and Innovation Programme under Grant Agreement N. 643238 (SYNCHRONICS). We also acknowledge the CARIPLO Foundation (IPER-LUCE No. 2015-0080) for funding. Computational work was supported by Supercomputing Laboratory at King Abdullah University of Science and Technology.

BA	*n*-butylammonium
MA	Methylammonium
SC-XRD	Single crystal X-ray diffraction
P-XRD	Powder X-ray diffraction
WAXS	Wide-angle X-ray scattering
DSC	Differential scanning calorimetry

[1] M. L. Petrus, J. Schlipf, C. Li, T. P. Gujar, N. Giesbrecht, P. Müller-Buschbaum, M. Thelakkat, T. Bein, S. Hüttner, and P. Docampo, Adv. Energy Mater. **7**, 1700264 (2017).
[2] S. Adjokatse, H.-H. Fang, and M. A. Loi, Mater. Today **20**, 413 (2017).
[3] H. Cho, S.-H. Jeong, M.-H. Park, Y.-H. Kim, C. Wolf, C.-L. Lee, J. H. Heo, A. Sadhanala, N. Myoung, S. Yoo, S. H. Im, R. H. Friend, and T.-W. Lee, Science **350**, 1222 (2015).
[4] X. Y. Chin, D. Cortecchia, J. Yin, A. Bruno, and C. Soci, Nat. Commun. **6**, 7383 (2015).
[5] M. D. Birowosuto, D. Cortecchia, W. Drozdowski, K. Brylew, W. Lachmanski, A. Bruno, and C. Soci, Sci. Rep. **6**, 37254 (2016).
[6] H. Wei, Y. Fang, P. Mulligan, W. Chuirazzi, H.-H. Fang, C. Wang, B. R. Ecker, Y. Gao, M. A. Loi, L. Cao, and J. Huang, Nat. Photonics **10**, 333 (2016).
[7] S. Yakunin, D. N. Dirin, Y. Shynkarenko, V. Morad, I. Cherniukh, O. Nazarenko, D. Kreil, T. Nauser, and M. V. Kovalenko, Nat. Photonics **10**, 585 (2016).
[8] B. Gholipour, G. Adamo, D. Cortecchia, H. N. S. Krishnamoorthy, M. D. Birowosuto, N. I. Zheludev, and C. Soci, Adv. Mater. **29**, 1604268 (2017).
[9] Y. Jia, R. A. Kerner, A. J. Grede, B. P. Rand, and N. C. Giebink, Nat. Photonics **11**, 784 (2017).
[10] B. R. Sutherland and E. H. Sargent, Nat. Photonics **10**, 295 (2016).
[11] W. Li, Z. Wang, F. Deschler, S. Gao, R. H. Friend, and A. K. Cheetham, Nat. Rev. Mater. **2**, 16099 (2017).
[12] T. Butler, F. Wang, M. Sabat, and C. L. Fraser, Mater. Chem. Front. **1**, 1804 (2017).
[13] B. Makowski, J. Kunzelman, and C. Weder, *Handbook of Stimuli-Responsive Materials* (Wiley-VCH Verlag GmbH & Co. KGaA, 2011), pp. 117.
[14] T. Mutai, H. Satou, and K. Araki, Nat. Mater. **4**, 685 (2005).
[15] M. Wuttig, H. Bhaskaran, and T. Taubner, Nat. Photonics **11**, 465 (2017).
[16] Z. Yang and S. Ramanathan, IEEE Photonics J. **7**, 1 (2015).
[17] J.-H. Lee, N. C. Bristowe, J. H. Lee, S.-H. Lee, P. D. Bristowe, A. K. Cheetham, and H. M. Jang, Chem. Mater. **28**, 4259 (2016).
[18] J. L. Knutson, J. D. Martin, and D. B. Mitzi, Inorg. Chem. **44**, 4699 (2005).
[19] M. E. Kamminga, G. A. de Wijs, R. W. A. Havenith, G. R. Blake, and T. T. M. Palstra, Inorg. Chem. **56**, 8408 (2017).
[20] D. Cortecchia, S. Neutzner, A. R. Srimath Kandada, E. Mosconi, D. Meggiolaro, F. De Angelis, C. Soci, and A. Petrozza, J. Am. Chem. Soc. **139**, 39 (2017).
[21] K.-Z. Du, Q. Tu, X. Zhang, Q. Han, J. Liu, S. Zauscher, and D. B. Mitzi, Inorg. Chem. **56**, 9291 (2017).
[22] J. S. Bechtel and A. Van der Ven, Phys. Rev. Mater. **2**, 025401 (2018).
[23] D. Cortecchia, C. Soci, M. Cametti, A. Petrozza, and J. Martí-Rujas, ChemPlusChem **82**, 681 (2017).
[24] P. S. Whitfield, N. Herron, W. E. Guise, K. Page, Y. Q. Cheng, I. Milas, and M. K. Crawford, Sci. Rep. **6**, 35685 (2016).
[25] A. N. Beecher, O. E. Semonin, J. M. Skelton, J. M. Frost, M. W. Terban, H. Zhai, A. Alatas, J. S. Owen, A. Walsh, and S. J. L. Billinge, ACS Energy Lett. **1**, 880 (2016).
[26] B. Saparov and D. B. Mitzi, Chem. Rev. **116**, 4558 (2016).
[27] M. D. Smith, A. Jaffe, E. R. Dohner, A. M. Lindenberg, and H. I. Karunadasa, Chem. Sci. **8**, 4497 (2017).
[28] L. Mao, Y. Wu, C. C. Stoumpos, B. Traore, C. Katan, J. Even, M. R. Wasielewski, and M. G. Kanatzidis, J. Am. Chem. Soc. **139**, 11956 (2017).
[29] L. Pedesseau, D. Sapori, B. Traore, R. Robles, H.-H. Fang, M. A. Loi, H. Tsai, W. Nie, J.-C. Blancon, A. Neukirch, S. Tretiak, A. D. Mohite, C. Katan, J. Even, and M. Kepenekian, ACS Nano **10**, 9776 (2016).
[30] H. Tsai, W. Nie, J.-C. Blancon, C. C. Stoumpos, R. Asadpour, B. Harutyunyan, A. J. Neukirch, R. Verduzco, J. J. Crochet, S. Tretiak, L. Pedesseau, J. Even, M. A. Alam, G. Gupta, J. Lou, P. M. Ajayan, M. J. Bedzyk, M. G. Kanatzidis, and A. D. Mohite, Nature **536**, 312 (2016).

[31] J.-C. Blancon, H. Tsai, W. Nie, C. C. Stoumpos, L. Pedesseau, C. Katan, M. Kepenekian, C. M. M. Soe, K. Appavoo, M. Y. Sfeir, S. Tretiak, P. M. Ajayan, M. G. Kanatzidis, J. Even, J. J. Crochet, and A. D. Mohite, Science **355**, 1288 (2017).
[32] G. Giorgi, K. Yamashita, and M. Palummo, J. Phys. Chem. Lett. **9**, 5891 (2018).
[33] D. B. Straus and C. R. Kagan, J. Phys. Chem. Lett. **9**, 1434 (2018).
[34] Q. Wang, X.-D. Liu, Y.-H. Qiu, K. Chen, L. Zhou, and Q.-Q. Wang, AIP Adv. **8**, 025108 (2018).
[35] O. Yaffe, A. Chernikov, Z. M. Norman, Y. Zhong, A. Velauthapillai, A. van der Zande, J. S. Owen, and T. F. Heinz, Phys. Rev. B **92**, 045414 (2015).
[36] Q. Zhang, L. Chu, F. Zhou, W. Ji, and G. Eda, Adv. Mater. **30**, 1704055 (2018).
[37] D. G. Billing and A. Lemmerer, Acta Crystallogr., Sect. B: Struct. Sci. **63**, 735 (2007).
[38] D. G. Billing and A. Lemmerer, New J. Chem. **32**, 1736 (2008).
[39] A. Lemmerer and D. G. Billing, Dalton Trans. **41**, 1146 (2012).
[40] A. Yangui, M. Sy, L. Li, Y. Abid, P. Naumov, and K. Boukheddaden, Sci. Rep. **5**, 16634 (2015).
[41] C. C. Stoumpos, D. H. Cao, D. J. Clark, J. Young, J. M. Rondinelli, J. I. Jang, J. T. Hupp, and M. G. Kanatzidis, Chem. Mater. **28**, 2852 (2016).
[42] K. Robinson, G. V. Gibbs, and P. H. Ribbe, Science **172**, 567 (1971).
[43] M. M. H. Smets, S. J. T. Brugman, E. R. H. van Eck, J. A. van den Ende, H. Meekes, and H. M. Cuppen, Cryst. Growth Des. **15**, 5157 (2015).
[44] S. Neutzner, F. Thouin, D. Cortecchia, A. Petrozza, C. Silva, and A. R. Srimath Kandada, Phys. Rev. Mater. **2**, 064605 (2018).
[45] F. Thouin, D. A. V. Chavez, C. Quarti, D. Cortecchia, I. Bargigia, D. Beljonne, A. Petrozza, C. Silva, and A. R. S. Kandada, e-print arXiv:1807.10539 (2018).
[46] F. Thouin, S. Neutzner, D. Cortecchia, V. A. Dragomir, C. Soci, T. Salim, Y. M. Lam, R. Leonelli, A. Petrozza, A. R. S. Kandada, and C. Silva, Phys. Rev. Mater. **2**, 034001 (2018).
[47] S. Meloni, G. Palermo, N. Ashari-Astani, M. Gratzel, and U. Rothlisberger, J. Mater. Chem. A **4**, 15997 (2016).
[48] R. Prasanna, A. Gold-Parker, T. Leijtens, B. Conings, A. Babayigit, H.-G. Boyen, M. F. Toney, and M. D. McGehee, J. Am. Chem. Soc. **139**, 11117 (2017).
[49] V. D'Innocenzo, G. Grancini, M. J. P. Alcocer, A. R. S. Kandada, S. D. Stranks, M. M. Lee, G. Lanzani, H. J. Snaith, and A. Petrozza, Nat. Commun. **5**, 3586 (2014).
[50] M. I. Dar, G. Jacopin, S. Meloni, A. Mattoni, N. Arora, A. Boziki, S. M. Zakeeruddin, U. Rothlisberger, and M. Grätzel, Sci. Adv. **2**, e1601156 (2016).
[51] C. Quarti, E. Mosconi, J. M. Ball, V. D'Innocenzo, C. Tao, S. Pathak, H. J. Snaith, A. Petrozza, and F. De Angelis, Energy Environ. Sci. **9**, 155 (2016).
[52] D. Cortecchia, J. Yin, A. Bruno, S.-Z. A. Lo, G. G. Gurzadyan, S. Mhaisalkar, J.-L. Brédas, and C. Soci, J. Mater. Chem. C **5**, 2771 (2017).
[53] J. Yin, H. Li, D. Cortecchia, C. Soci, and J.-L. Brédas, ACS Energy Lett. **2**, 417 (2017).
[54] E. P. Booker, T. H. Thomas, C. Quarti, M. R. Stanton, C. D. Dashwood, A. J. Gillett, J. M. Richter, A. J. Pearson, N. J. L. K. Davis, H. Sirringhaus, M. B. Price, N. C. Greenham, D. Beljonne, S. E. Dutton, and F. Deschler, J. Am. Chem. Soc. **139**, 18632 (2017).
[55] D. Cortecchia, K. C. Lew, J.-K. So, A. Bruno, and C. Soci, Chem. Mater. **29**, 10088 (2017).
[56] S. Neutzner, A. R. S. Kandada, G. Lanzani, and A. Petrozza, J. Mater. Chem. C **4**, 4630 (2016).
[57] M. Li, Q. Gao, P. Liu, Q. Liao, H. Zhang, J. Yao, W. Hu, Y. Wu, and H. Fu, Adv. Funct. Mater. **28**, 1707006 (2018).